Advances in Concrete Construction, *Vol. 1, No. 2 (2013) 121-136*
DOI: http://dx.doi.org/10.12989/acc.2013.1.2.121

Effect of corrosion pattern on the ductility of tensile reinforcement extracted from a 26-year-old corroded beam

Wenjun Zhu and Raoul François*

Université de Toulouse, UPS, INSA, LMDC (Laboratoire Matériaux et Durabilité des Constructions), Toulouse, France

(Received November23, 2012, Revised February 25, 2013, Accepted April 18, 2013)

Abstract. Tension tests were carried out to investigate the effect of the corrosion pattern on the ductility of tension bars extracted from a 26-year-old corroded reinforced concrete beam. The tensile behavior of corroded bars with different corrosion patterns was examined carefully, as were two non-corroded bars extracted from a 26-year-old control beam. The results show that corrosion leads to an increase in the ratio of the ultimate strength over the yield strength, but reduces the ultimate strain at maximum force of the reinforcement. Both the corrosion pattern and the corrosion intensity play an important role in the ductile properties. The asymmetrical distribution of the corrosion around the surface is a decisive factor, which can influence the ultimate strain at maximum force more seriously.

Keywords: corrosion; tensiontest; ductility; ultimate elongation; steel bar

1. Introduction

The corrosion of reinforcement, which commonly happens in a chloride environment, is considered to be one of the major problems for the deterioration of reinforced concrete structures, which has been the object of great attention from both researchers and engineers (Care *et al.* 2008, Zhu *et al.* 2012, Bhargavak *et al.* 2006). Corrosion damage of the reinforcement can not only reduce the cross-section of the steel bar but also produce stress in the concrete around the bar which can gradually result in cracking or even spalling of the concrete cover as the volume of the corrosion products increases (Wong *et al.* 2010). Considerable resources are expended to repair and rehabilitate deteriorating concrete structures (Kreit *et al.*). It has been reported that, in the USA, such repair and rehabilitation costs over $20 billion per year (Strategic High Research Program 1989).

Much research work has been done to deal with this corrosion problem, especially the corrosion of reinforcement. Ahmad (2003) has reviewed reinforcement corrosion in concrete structures and assessed the causes and extent of corrosion of reinforcements, so as to predict the residual behavior of a corroded structure exposed to an aggressive environment. Apostolopoulos *et al*. (2006) have noted the increase in steel stress at corroded cross-sections, and also observed reduction of the ductility. Stewart (2009), Maslehuddin *et al*. (1990) have also investigated the

*Corresponding author, Professor, E-mail: raoul.francois@insa-toulouse.fr

http://www.techno-press.org/?journal=acc&subpage=7 ISSN:2287-5301(Print)2287-531X(Online)

influence of corrosion on the mechanical properties of the reinforcement in different conditions. However, most research has concentrated on the yield strength and ultimate strength based on the nominal diameter without considering the loss of cross-section due to corrosion (Lee and Cho 2009, Palsson and Mirza 2002). In fact, relatively less work has been done on natural corrosion and the ductility of corroded bars (Coronelli and Gambarova 2004). The ductility of the reinforcement and the minimum cross-section of the tension bars are the two key elements that determine the ductile behavior of corroded RC structures.

Along-term program on the corrosion of RC beams in a chloride environment under service load (Zhang and Castel 2009) has been carried out since 1984, at Laboratoire Matériauxet Durabilité des Constructions (L.M.D.C.) in Toulouse, in southwest France. In this program, the corrosion response of the beams has been investigated, from crack development to mechanical performance (Zhu and François 2012, Vidal *et al.* 2004). The experiments presented in this paper are based on this program. The tension bars are extracted from both corroded and control beams and tension tests are carried out on the bars. The goal of this work is to find the relationship between the corrosion level and the ductility of highly corroded bars.

2. Experimental program

The intention of this program was to further understand the steel corrosion process in concrete elements and the impact of corrosion on the mechanical behavior. Thirty-six RC beams were cast with dimensions 3000 × 280 × 150 mm, which were widely used in the construction industry at that time. The beams were classified in group A or group B according to the diameter of the steel bars and the depth of the concrete cover. Then they were transferred into a chloride environment under two kinds of service load. Another 36 RC beams with the same composition and configuration were cast as a control group. The control beams were also under service load but were all kept in an ordinary laboratory room rather than in an aggressive chloride environment. In this way, the influence of chloride corrosion could be studied by comparing the corroded beams and the control beams. A series of works have been published at different stages of this long-term program, the content of which covers crack development, chloride content, and mechanical response (Coronelli and Gambarova 2004, Zhang *et al.* 2009, Zhu and François 2012, Vidal *et al.* 2004, Khan *et al*. 2011).

In this paper, the focus will be on the mechanical properties of the corroded tension bars. All the bars are extracted from the tensile reinforcement of two 26-year-old beams: a corroded B2Cl2 and a control B2T, where B stands for beams in group B, B2 means the second load level, Cl stands for the corroded beams, T means the control beams (non-corroded beams).

Table 1 Concrete composition

Mix composition							
Rolled gravel (silica + limestone)					5/15 mm		1220 kg/m^3
Sand					0/5 mm		820 kg/m^3
Portland cement: OPC HP (high perform)							400 kg/m^3
Water							200 kg/m^3
Cement composition	SiO_2	Al_2O_3	Fe_2O_3	CaO	MgO	SO_3	Na_2O
Weight (%)	21.4	6.0	2.3	63.0	1.4	3.0	0.5

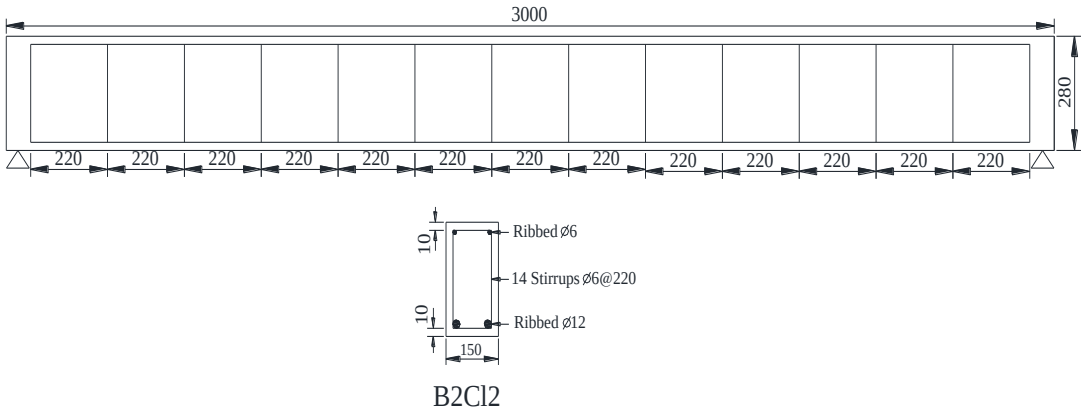

Fig. 1 Layout of the reinforcement for the beam (mm)

2.1 Concrete composition

The composition of the concrete and the cement is shown in Table 1. The water: cement ratio was 0.5. However, the exact value was adjusted so as to meet the constant workability requirement of 70 mm in the slump test.

2.2 Material properties

The concrete properties were determined by testing cylindrical specimens of diameter 110 mm and height 220 mm at 28 days. The average compressive stress was 45 MPa, and the elastic modulus was about 32 GPa. The tensile strength was 4.7 MPa which was got from splitting test. The porosity of the concrete was about 15.2%. For all the steel bars, the nominal yield strength was 500 MPa.

2.3 Reinforcement layout

The configuration of the beams (group B) is shown in Fig. 1. The concrete cover was 10 mm thick, which corresponds to the minimum depth in a non-aggressive environment according to French regulations (B.A.E.L. 1983) at the time of casting.

2.4 Loading system

All the beams were loaded in a three-point loading system by placing a Group B beam above a Group A beam as shown in Fig. 2. Two levels of load were applied. The bars studied in this paper were from beam B2Cl2, and were designed to support a moment of 21.2 kN·m at the mid-span, which corresponded to 80% of the failure load and twice the design service load in the aggressive environment according to the French standard of the time. It should be noticed that ULS design of B beams was also in accordance in term of load level with current standard (EC2), only the concrete cover would be increased to 20 mm in current standard. The maximum stress in the tension bars, σ_s, was considered to be 380MPa.

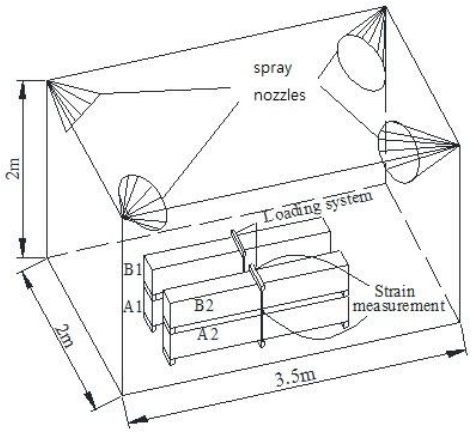

Fig. 2 Loading system and chloride environment

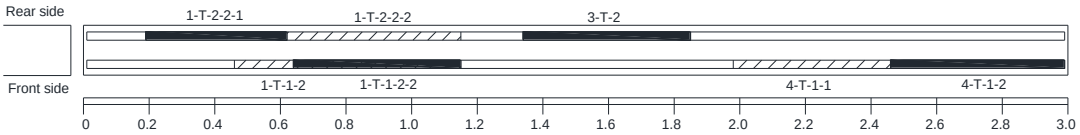

B2CL2--location of the tensile test samples

Fig. 3 Locations of the tension samples

2.5 Conservation environment

After all the corroded beams had been put together as described above, they were transferred to the chloride environment. As shown in Fig. 2, the salt fog was generated in the confined room by four sprays located in the upper corners. It was made using a solution of 3% NaCl, the same salt concentration as in sea water. The conservation environment was:

0-6 years: cycles of 15 drying days and 7 wetting days under laboratory conditions ($T \approx 20$℃).

6-9 years: cycles of 7 drying days and 7 wetting days under laboratory conditions ($T \approx 20$℃).

9-19 years: cycles of 7 drying days and 7 wetting days, but the beams were transferred outside, the beams were exposed to the temperature of southwest of France (average value per month from 5℃ to 21℃).

19-23 years: cycles have been stopped and the beams were unloaded in the outside.

At the same time, all the control beams were kept in a laboratory room with an R.H. of 50%, and at a temperature of 20℃ throughout the experiment.

3. Results and discussion

After 26 years, the corroded beam B2Cl2 from the aggressive environment and the control beam B2T were broken to provide access to the tension bars of both beams. Then seven samples were taken from different parts of the two tension bars as shown in Fig. 3. The details of the corroded and non-corroded samples are shown in Table 2. The length of effective range is the distance between fixed points of LVDT, and it is shown in Fig. 4.

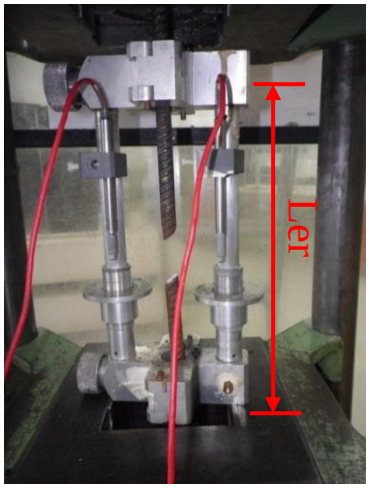

Fig. 4 Uniaxial tension tests on the bars

Table 2 Details of the tension bars

	Location	Label	Length of sample (mm)	Length ofeffective range (mm)	Mass (g)	Mass/meter of length (g/m)
Corroded bars	Front side	1-T-1-2	662.58	201	512.25	772.9
	Front side	1-T-1-2-2	479.22	201	374.43	780.5
	Front side	4-T-1-1	615.76	201	480.78	780.8
	Front side	4-T-1-2	509.86	230	411.21	806.5
	Rear side	1-T-2-2-1	447.02	224	359.70	804.7
	Rear side	1-T-2-2-2	487.10	216	402.12	825.5
	Rear side	3-T-2	430.80	201	334.14	775.6
Non-corroded bars	Front side	B2T-1-2	580	200	510.65	887.8
	Rear side	B2T-2-2	557	201	493.04	887.8

A 250-kN-capacity machine was used to carry out the tension test as shown in Fig. 4. Two LVDTs distant of about 200 mm (Ler) measured the elongation of the tension bar. The tensile properties of the bars were calculated from the results of the tensile test.

3.1 Corrosion distribution

The corroded tension bars were put into Clarke's Solution ANSI/ASTM G1-72 to clean the corrosion products from the steel. Then the corrosion distribution was drawn in pitting corrosion and general corrosion (Fig. 6) from the top view and bottom view as shown in Fig. 5(b).

3.2 Loss of cross-section of the corroded tension samples

After the tension test, the tension samples were cut into small pieces so that the average mass loss of the tension bars could be determined. The length of the small pieces depended on the corrosion pattern and the corrosion distribution which was shown in Fig. 5(a). The aim was to make sure that the residual mass of the steel was uniform throughout the length of each piece. The shortest length could be less than 5 mm. It should be pointed out that the plastic residual

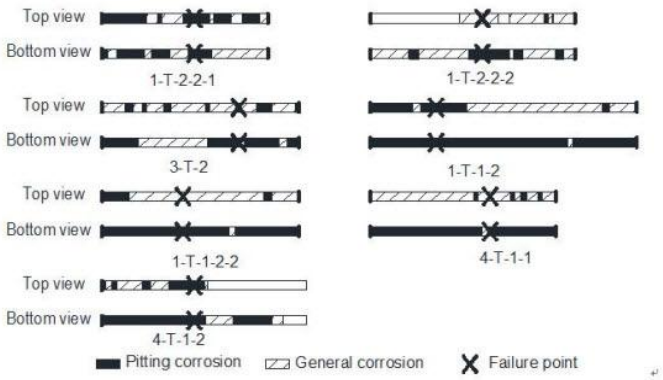

(a) Corrosion distribution in the tension samples

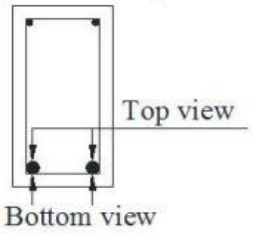

(b) Two directions of viewing

Fig. 5 Corrosion distribution

deformation of the corroded bars during the tension test was assumed to be very limited due to the brittle failure.

The nominal mass of the steel bars can be calculated by Eq. (1). The mass loss of the small pieces of the corroded bars was measured and the loss of cross-section was calculated from the loss of mass by Eq. (2)

$$m_0 = \rho \cdot A_s \cdot L \tag{1}$$

$$\Delta A_s = \frac{m_0 - m}{m_0} \cdot A_s \tag{2}$$

Where: ρ (g/cm^3) is the density of the steel bars, considered to be 7.85 g/cm^3.

L (mm) is the length of each piece of the steel bars, measured with a vernier caliper.

ΔAs (mm^2) is the average cross-section loss of the small piece of bar.

As (mm^2) is the nominal cross-section of the steel bars.

m (g) is the residual mass of the small pieces of the corroded bars.

m_0 (g) is the nominal mass of the steel bars.

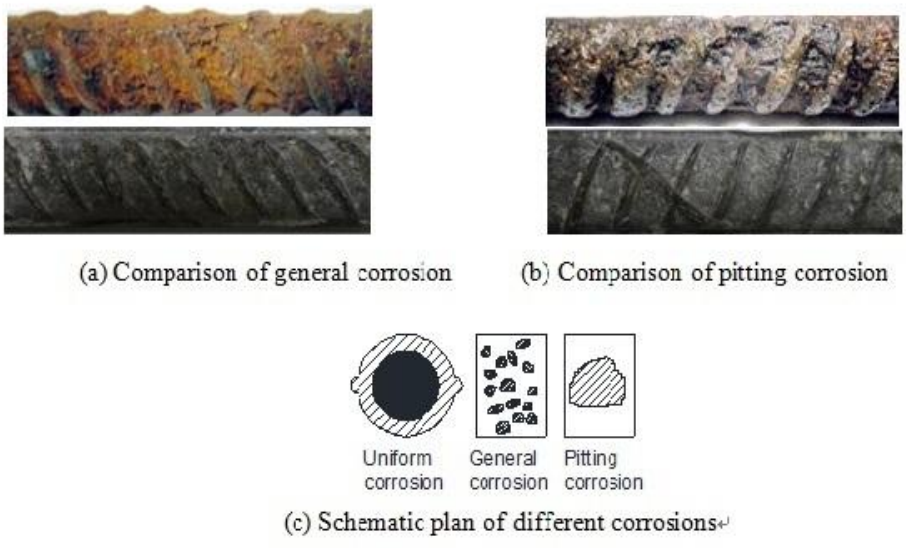

Fig. 6 General corrosion and pitting corrosion of the bars

4. Experimental results

4.1 Loss of cross-section of the corroded bars

As shown in Fig. 5, the corrosion distribution was different according to the viewing direction. However, because of the long duration of exposure to the chloride environment, corrosion had developed along almost the whole length of the samples. The corrosion distribution was not uniform, neither in pattern nor in corrosion level. Pitting corrosion referred to large local loss of cross-section and general corrosion referred to a cluster of small pits (Fig. 6). Both general and pitting corrosion existed on most surfaces of the corroded bars. Nevertheless, pitting corrosion was more serious in the bottom view than the top view, which was due to the smaller depth of the concrete cover and the fact that corrosion induced by natural processes was not uniform. It should be pointed out that the greatest loss of cross-section corresponded to pitting corrosion. Then, the failure point during tension tests was always located in a general corrosion zone with serious pitting depth.

As shown in Fig. 7, the loss of cross-section appeared practically throughout the length of the corroded bars. The maximum loss of cross-section reached as much as 56 mm^2 for the samples from the front side tension bar and 51 mm^2 for the samples of the rear side tension bar. It should be noted that, along tension bars, the variation of the loss of cross-section was very significant, reaching 50% of the initial cross-section in places, and failure always occurred at the location with maximum pitting corrosion.

4.2 Tension tests

The stress and strain curves for the tension bars are shown in Fig. 8. The stress was calculated

by the force and the effective cross-section at the failure point, while the strain was deduced from the average deformation over the effective length Ler of about 200 mm. Indeed, as the failure location was unknown, it was impossible to choose a given short length of bar to measure the deformation. However, the inconsistency between local stress and global strain calculations was acceptable since the change in elongation beyond the yielding stress was due to necking in the failure zone of control steel bar and it was the change in failure mode from ductile behavior with necking to brittle behavior without necking which reduced the corroded steel elongation. This change was of cause evaluated for a given based length, but it would not significantly be modified with a change in based length.

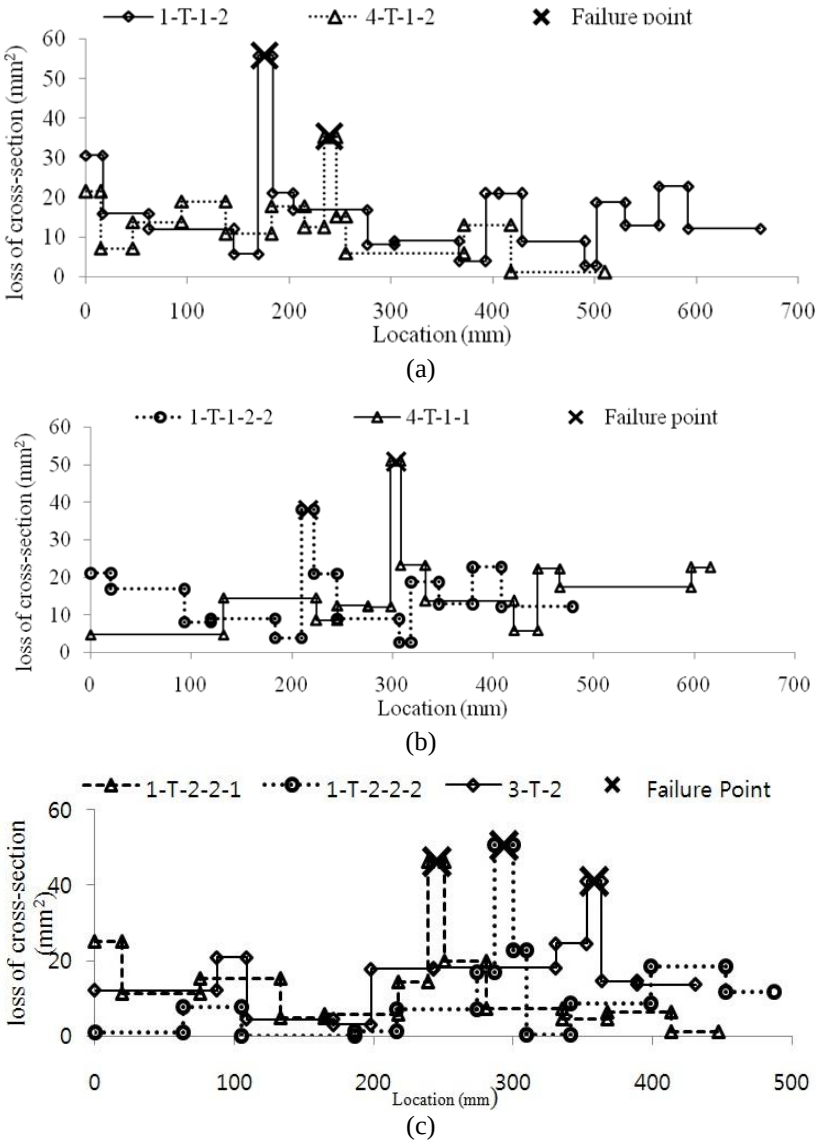

Fig. 7 Loss of cross-section of the corroded tension bars

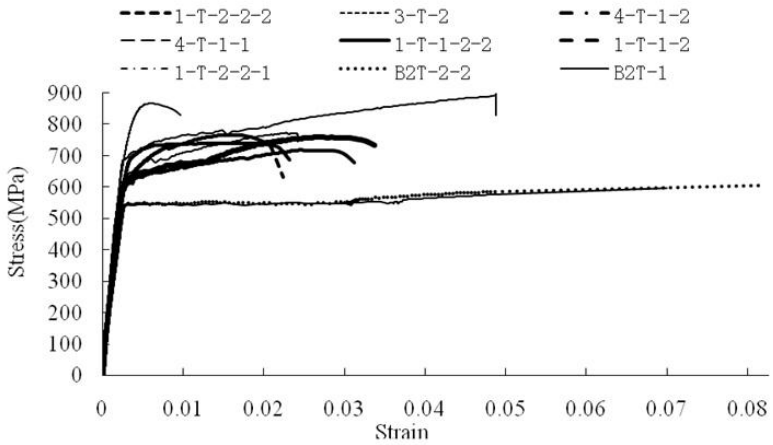

Fig. 8 Stress-strain curves of the tension tests

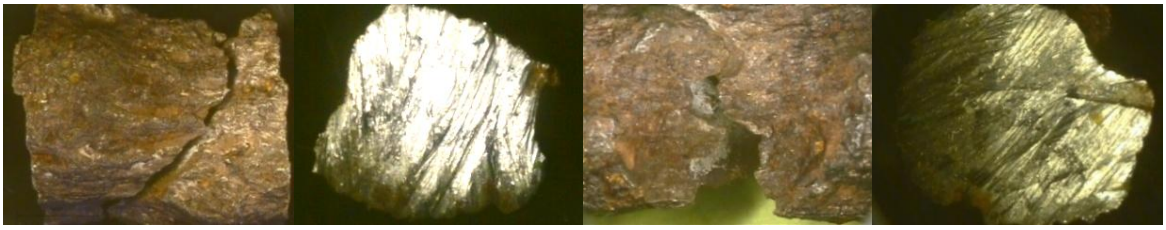

(a) 4-T-1-1 (b) 1-T-1-2

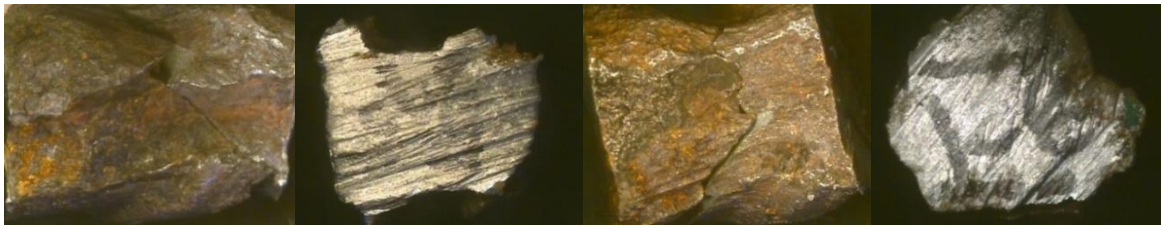

(c) 1-T-2-2-2 (d) 1-T-2-2-1

Fig. 9 Corrosion distribution in the cross-section at failure point

Fig. 10 Failure point of the non-corroded bar B2T-1-2 with necking phenomena

The shape of tensile test curve for corroded bars differed from the curve for the control bar in that, like diagrams for cold-formed steel, they lacked a well-defined yield point. Then yield stress in calculated as 0.2% proof strain.

The curves for the nine bars were not identical (Fig. 8). The ductility of the corroded bars appears to be strongly reduced, but both the yield stress and the ultimate stress of the corroded bars increased in comparison with the non-corroded bars.

5. Properties of the corroded bars

5.1 Residual cross-section of the failure points

The failure points of the steel bars were sawed carefully so that their mechanical properties could be investigated more effectively. All the failure points of the steel samples are shown in Figs. 9 and 10. The failure points of the corroded bars occurred at locations with serious pitting corrosion.

Figs. 9 and 10 show that, in comparison with the non-corroded bars, most of the corroded bars had at least one obvious groove corresponding to corrosion pits. As a result, the cross-section of the corroded bars was no longer circular, which made it rather complicated to measure. So the cross-section of the corroded bars was calculated from the residual mass measured on small pieces, which was considered to give a closer estimate of the true residual cross-section than the residual diameter measured using a vernier caliper. The corroded bars showed much smaller elongation at fracture location during the tension test and exhibited more brittle behavior than the non-corroded bars, which were ductile and showed necking at failure (Fig. 10).

5.2 Characteristics of the steel bars

In this section, the ductility of the corroded bars will be discussed on the basis of the experimental results. The loss of cross-section and the pit depth of the corroded bars at the failure point will be considered as the main factors. According to Eurocode 2 (BS EN 1992) the reinforcement should have adequate ductility as defined by the ratio of the tension strength to the yield strength, f_u/f_y, and the elongation at maximum force, ε_{uk} (ultimate strain), indicated in Table 3.

The properties of the steel bars are shown in Table 4. In comparison with the non-corroded bars, the properties of the corroded bars had been changed tremendously, including the yield strength, the ultimate strength and the ratio f_u/f_y, the ultimate strain at maximum load ε_u.

The yield strength was about 530 MPa for the non-corroded bars as shown in Table 4, which was slightly higher than the nominal value but still in the 400-600 MPa range defined by Eurocode 2

Table 3 Properties of reinforcement according to Eurocode 2

Product form	Bars and de-coiled rods		
Class	A	B	C
Characteristic yield strength f_{yk} (MPa)		400 to 600	
Minimum value of f_u/f_y	≥1.05	≥1.08	≥1.15 and ≤1.35
Characteristic strain at maximum force, ε_{uk} (%)	≥2.5	≥5.0	≥7.5

However, for the corroded bars, the yield strength ranged from 580 MPa to 750 MPa. The corrosion had significantly influenced the yield strength of the bars, which finally appeared to be outside the range prescribed by Eurocode 2 as defined in Table 3. For the ultimate strength and the ratio of f_u/f_y, all the values of the corroded bars were over the non-corroded bars. The reason could be due to the different deformation performance of the corroded bars and the non-corroded bars and the cross-section which was adopted for the calculation of the stress.

As discussed before, necking behavior was the most significant factor between the corroded bars and non-corroded bars when the bars reached yield strength. The residual cross-section was adopted for the corroded bars. As the corroded bars showed brittle response, there was almost no necking then the use of the residual cross-section allowed a good approximation of ultimate stress. But, for the non-corroded bars, the necking could not be ignored. However, the cross-section used in the calculation of stress was the nominal one which was correct for yield stress, but would resulted in underestimating the effective ultimate stress due to the necking with reduce the effective cross-section at failure. In order to take into account of this necking effect, 20% reduction was considered as a first approach for the residual cross-section of the non-corroded bars. Then in the following discussion, they would be treated as nominal ultimate strength f_u (without reduction) and effective ultimate strength f_{ue} (with reduction) respectively. At the same time, the nominal value of the non-corroded bars could stand for the limit of pure brittle behavior of the tension tests, while the effective value could be considered as the ductile response.

5.3 Effect of corrosion on the ratio of tensile strength to yield strength (f_u/f_y) and ultimate strain (ε_u)

Fig. 11 shows the relationship between the ratio of ultimate tensile strength and yield strength including (f_u/f_y and f_{ue}/f_y) and the loss of cross-section. For the corroded bars, the value f_u/f_y was really in scattered distribution and no law could be drawn. All the results ranged from Class B to class C. Meanwhile, the results of the corroded bars were also between the nominal ratio (f_u/f_y) and the effective ratio (f_{ue}/f_y) of the non-corroded bars.

Fig. 12 shows that the ultimate strain ε_u is reduced in relation with loss of cross-section due to corrosion. For the non-corroded bars, the ultimate strain corresponds at least to Class B while, for the corroded bars, the ultimate strain was mostly below the Class A threshold. Even though some

Table 4 Properties of the steel bars calculated from the tension test

	Samples	Yield strength f_y (MPa)	Ultimate strength f_u (MPa)	Ultimate strength f_{ue} (MPa)	f_u/f_y	f_{ue}/f_y	Ultimate strain at maximum force ε_u (%)
Corroded bars	1-T-1-2	601	717		1.19		2.5
	1-T-1-2-2	670	740		1.10		1.5
	4-T-1-1	687	890		1.30		4.8
	4-T-1-2	618	760		1.23		2.7
	1-T-2-2-1	750	854		1.14		0.6
	1-T-2-2-2	580	766		1.32		1.6
	3-T-2	628	772		1.23		2.28
Non-corroded bars	B2T-1-2	532	592	710	1.11	1.33	7.0
	B2T-2-2	539	601	721	1.12	1.34	8.2

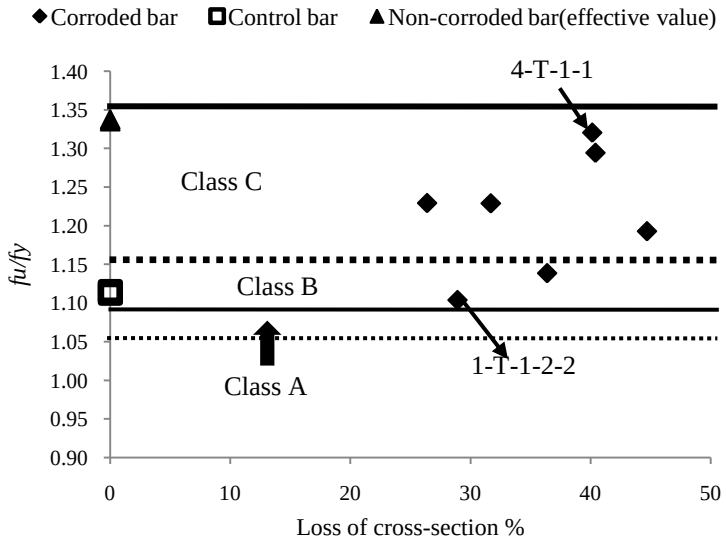

Fig. 11 Ratio of ultimate stress to yield stress of the steel bars

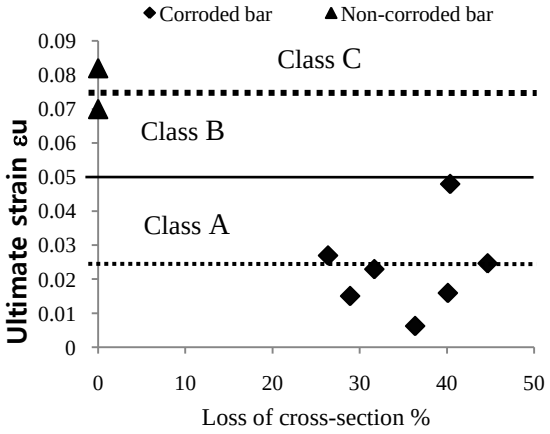

Fig. 12 Ultimate strain of the steel bars

of the results were higher than the Class A threshold, the residual ductility of the corroded bars was not sufficient according to Table 3. In Table 4, all the corroded bars had stronger yield strength and ultimate strength than that of the non-corroded bars, but over half of the corroded bars' ultimate strain was too weak to reach the threshold value of 2.5%, which meant that ductility would be the determinant factor for highly corroded bars, and the brittle behavior of the steel bars would require special attention to assess the quality of the existence corroded structures.

5.4 Relation between loss of cross-section and ultimate strain at maximum force (ε_u)

Castel *et al*. (2000) carried out tension tests on notched re-bars, which showed a significant reduction in ductility. They proposed a model of corroded bar behavior (Eq. (4)) between the loss

of cross-section and the ratio of ultimate elongation of corroded bar to ultimate elongation of a control bar.

$$\frac{\varepsilon_{ucorr}}{\varepsilon_u} = e^{-0.1c\%} \tag{3}$$

But the value should not be less than 0.2.

Cairns *et al*. (2005) also conducted research on both the effect of notches in steel bars (marked as results 1) and steel damage due to an accelerated corrosion process (marked as results 2). In order to compare the results of Castel *et al*. (2000) and Cairns *et al*. (2005)'s tests, the curve of the relative ultimate strain versus the loss of cross-section is plotted in Fig. 13.

According to Fig. 13, Cairns' results 2 match Castel's model well. Nevertheless, Cairns' results 1 were above Castel's model, but the results supported the proposal that the minimum ratio of the relative ultimate strain should be 0.2. The experimental results presented in this paper were also compared with Castel's model. They appeared generally conservative, which was logical since notches had a constant shape, unlike real pits, which could be more or less pointed as shown in Fig. 14. Thus, the damage/reference ultimate strain ratio for corroded bar 1-T-2-2-1 was below 0.2 but was almost 0.7 for 4-T-1-1.

5.5 Effect of cross-section corrosion pattern on ductility of steel bar

Corrosion led to a decrease in the ultimate elongation but there was high scatter on the loss of cross-section and the depth of pitting corrosion of steel bars. The explanation could be that the

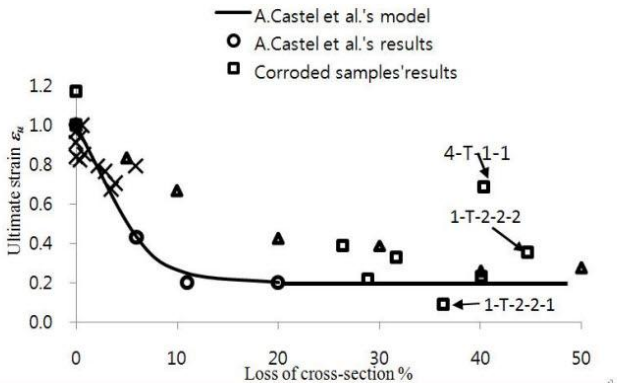

Fig. 13 Evolution of ultimate strain at maximum force versus the steel cross-section reduction

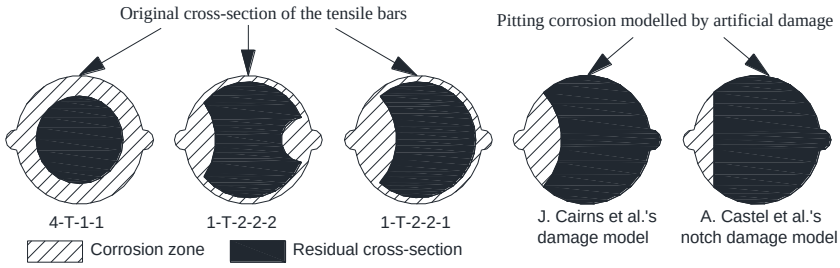

Fig. 14 Corrosion distribution in the cross-section at failure point

cross-sectional corrosion pattern at the failure point was very variable. The corrosion pattern of 1-T-2-2-1 was the sharpest, as shown in Fig. 14. A huge corrosion pit appeared in only one side of the steel bar while, for other bars, the corrosion was more or less distributed all around the perimeter of the cross-section (e.g., for sample 4-T-1-1), so the ultimate strain was the highest of all the corroded bars. Castel's model was built using notched re-bars. The residual cross-sections were highly asymmetric and close to sample 1-T-2-2-1.This would result in an eccentricity of the center of gravity of the cross-section to the force axis, which could induce local bending and reduce the ultimate strain, and then lead to conservative results.

The shape and distribution of pitting corrosion in a steel cross-section would play a very important role in the reduction of ultimate elongation. Sharper, deeper pitting corrosion would lead to more pronounced concentration for the strain and stress and more brittle failure would occur. Stress concentration led to partial yielding of the cross-section and, according to the fracture mechanics theory, when the whole cross-section of the steel bar reached the elastic limit, a large part of yielding reserve had already been consumed, which led to premature rupture of the bar (Castel *et al.* 2000, Cairns *et al.* 2005, Almusallam 2001). However, it was worth noting that the effect of such asymmetry would be less significant for a bar embedded in concrete than one tested in air. As the corrosion products could fill into the corrosion zones, the bond and constraint from the concrete around the bar could make some contribution to the mechanical performance.

An equivalent steel concept (Cosenza *et al.* 1998) was defined to judge the overall steel ductility. Nevertheless, because of the large scatter on the value of effective cross-section after corrosion and then high yield stress recorded, the use of this concept would not be useful because due to antagonist evolution of yield stress with corrosion and ultimate strain.

5.6 Global mechanical behavior of the corroded beam B2Cl2 and control beam B2T

The mechanical behavior of beam B2Cl2, with the corroded bars, and the non-corroded beam B2T are shown in Fig. 15. Both the yielding capacity and the ultimate capacity of beam B2Cl2 were reduced significantly by the corrosion of the steel bars, these trends agreed well with the tension results of the corroded bars in Fig. 8. However, the ratio of ultimate capacity to yield capacity, F_u/F_y, for non-corroded beam B2T was 1.12. While the ratio of ultimate capacity to yield

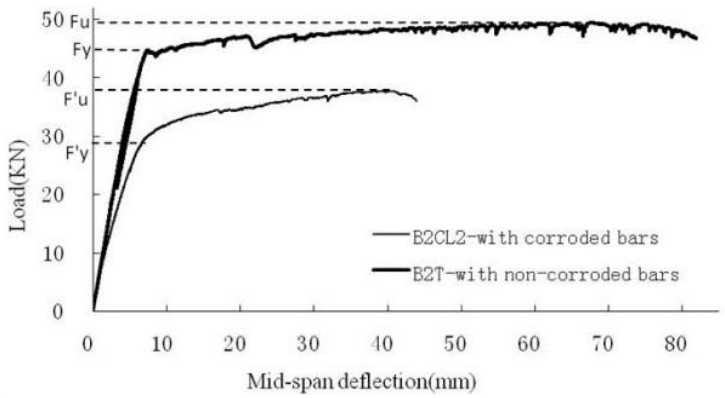

Fig. 15 Force-deflection curves for the beam

capacity for the corroded beam B2Cl2, F'_u/F'_y, was 1.25, much higher than that of the non-corroded beam. Thus, the difference in post-yielding behavior found on steel bars led to a modification of the post yielding performance of the corroded beam

The ductility of the beam was also greatly reduced, almost to half of that of the non-corroded beam, which was more serious than the reduction of the capacity. The ratio of ultimate deflection between the corroded beam B2Cl2 and non-corroded beam B2T, D/D', was 53.6%, which means that the deflection of the corroded beam was almost half that of the non-corroded beam.

6. Conclusions

Tension tests were carried out on seven steel bars with different levels of corrosion and two non-corroded bars extracted from two 26-year-old beams to investigate the mechanical behavior of corroded steel bars. The ratio of the tensile strength to the yield stress and the ultimate strain at maximum force (ultimate strain) were studied in relation to the loss of cross-section. In order to better understand the mechanical behavior, the shapes of the cross-sections at the failure points of the tension bars were analyzed carefully. Yield stress of corroded bars increased deeply and the scatter on the measurement of the effective cross-section was not enough to explain it. More research was needed to understand these results which could be influence by the steel bar diameter. Indeed, a 16 mm diameter used in François *et al.* showed a weakest increase in yield stress. Ultimate stress increased also sharply for corroded steel, but the comparison with non-corroded steel was complex due to a strong reduction of necking phenomena for corroded bars.

The ultimate strain of steel bars was reduced greatly by corrosion. These results agreed with the model by Castel *et al*. although the model was relatively conservative due to the fact that it was built from results obtained with an artificial notch rather than natural pitting corrosion. The loss of cross-section and the depth of the pitting corrosion were found to be less important than the shape of the corrosion in the cross-section, which was considered to be the decisive factor for the ductile behavior of the corroded bars. When the corrosion was distributed uniformly around the cross-section, the steel bar exhibited good ductility. Nevertheless, when the pitting corrosion occurred asymmetrically around the cross-section, the steel bar responded with more brittle behavior.

Although both the yield stress and ultimate stress of all the corroded bars were improved, the ductility of most of the corroded bars decreased below the threshold fixed by Eurocode 2. This result showed that the residual ultimate elongation of a corroded steel bar might be the most important parameter effecting reliability as far as the structural performance of an RC structure damaged by corrosion in a chloride environment was concerned.

References

Ahmad, S. (2003), "Reinforcement corrosion in concrete structures, its monitoring and service life prediction-a review", *Cem. Concr. Composit.*, **25**(4-5), 459-471.

Almusallam, A.A. (2001), "Effect of degree of corrosion on the properties of reinforcing steel bars", *Construct Build Mater*, **15**(8), 361-368.

Apostolopous, C.A., Papadopoulus, M.P. and Pantelakis, S.G. (2006), "Tensile behavior of corroded reinforcing steel bars BSt 500s", *Construct. Build. Mater.*, **20**(9), 782-789.

B.A.E.L. (1983), French regulations for reinforced concrete structures.

Bhargava, K., Ghosh, A.K., Mori, Y. and Ramanujam, S. (2006), "Model for cover cracking due to rebar corrosion in RC structures", *Eng. Struct.*, **28**(8), 1093-1109.
BS EN 1992-1-1 Eurocode 2, Design of concrete structures-Part 1-1: General rules and rules for buildings, October 2005.
Cairns, J., Plizzari, G.A., Du, Y.G., Law, D.W. and Franzoni, C. (2005), "Mechanical properties of corrosion-damaged reinforcement", *ACI Mater. J.*, **102**(4), 256-264.
Caré, S., Nguyen, Q.T., L'hostis, V. and Berthaud, Y. (2008), "Mechanical properties of the rust layer induced by impressed current method in reinforced mortar", *Cem. Concr. Res.*, **38**(8), 1079-1091.
Castel, A., François, R. and Arligue, G. (2000), "Mechanical behaviour of corroded reinforced concrete beams—Part 2: Bond and notch effects", *Mater. Struct.*, **33**(9), 545-551.
Coronelli, D. and Gambarova, P. (2004), "Structural assessment of corroded reinforced concrete beams: modeling guidelines", *J. Struct. Eng. ASCE*, **130**(8), 1214-1224.
Cosenza, E., Greco, C. and Manfredi, G. (1998), *An Equivalent steel Index in the Assessment of ductility Performances of the Reinforcement*, CEB Bulletin No. 242.
François, R., Khan, I. and Dang, V.H. (2013), "Impact of corrosion on mechanical properties of steel embedded in 27-year-old corroded reinforced concrete beams", *Mater. Struct.*, **46**(6), 899-910.
Khan, I., François, R. and Castel, A. (2011), "Mechanical behavior of long-term corroded reinforced concrete beam", *Model. Corr. Conc. Struct.*, **5**(10), 243-258.
Kreit, A., Al-Mahmoud, F., Castel, A. and François, R.(2011), "Repairing corroded RC beam with near-surface mounted CFRP rods", *Mater. Struct.*, **44**(7), 1205-1217.
Lee, H.S. and Cho, Y.S. (2009), "Evaluation of the mechanical properties of steel reinforcement embedded in concrete specimen as a function of the degree of reinforcement corrosion", *Int. J. Frat.*, **157**(1-2), 81-88.
Maslehuddin, M., Ibrahim, I.M., Al-Sulaimani, G.J., Al-Mana, A. and Abduljauwad, S.N. (1990), "Effect of rusting of reinforcing steel on its mechanical properties and bond with concrete", *ACI Mater. J.*, **87**(5), 496-502.
Palsson, R. and Mirza, M.S. (2002), "Mechanical response of corroded steel reinforcement of abandoned concrete bridge", *ACI Struct. J.*, **99**(2), 157-162.
Stewart, M.G. (2009), "Mechanical behaviour of pitting corrosion of flexural and shear reinforcement and its effect on structural reliability of corroding RC beams", *Struct. Safety*, **31**(1), 19-30.
Strategic High Research Program (1989), *Concrete and structure: Progress and product update*, Washington DC, National Research Council.
Vidal, T., Castel, A. and François, R. (2004), "Analyzing crack width to predict corrosion in reinforced concrete", *Cem. Concr. Res.*, **34**(1), 165-174.
Wong, H.S., Zhao, Y.X., Karimi, A.R. and Jin, W.L. (2010), "On the penetration of corrosion products from reinforcing steel into concrete due to chloride-induced corrosion", *Corros. Sci.*, **52**(7), 2469-2480.
Zhang, R.J., Castel, A. and François, R. (2009), "The corrosion pattern of reinforcement and its influence on serviceability of reinforced concrete members in chloride environment", *Cem. Concr. Res.*, **39**(11), 1077-1086.
Zhu, W.J. and François, R. (2012), "Corrosion of the reinforcement and its influence on the residual structural performance of a 26-year-old corroded RC beam", *Proceeding of the 3rd International Conference on Concrete Repair, Rehabilitation and Retrofitting*, Cape Town, South Africa, September.
Zhu, W.J., François, R. and Coronelli, D. (2012), "Effect of corrosion of reinforcement on the coupled shear and bending behaviour of reinforced concrete beam", *Proceeding of the 6th International Conference on Bridge Maintenance*, Safety and Management, Stresa, Lake Maggiore, Italy, July.

JK